Water Supply

IWA PUBLISHING

Water Supply Vol 22 No 5, 5095 doi: 10.2166/ws.2022.162

Location identification of river bathymetric error based on the forward and reverse flow routing

Jiabiao Wang [a], Xiaohui Lei[b], Siyu Cai[b] and Jianshi Zhao[c,*]

[a] School of Civil Engineering, Sun Yat-Sen University, Zhuhai 519082, China
[b] China Institute of Water Resources and Hydropower Research, Beijing 100038, China
[c] Tsinghua University, Beijing 100084, China
*Corresponding author. E-mail: zhaojianshi@tsinghua.edu.cn

JW, 0000-0002-0399-0164

ABSTRACT

River bathymetric data is fundamental to water flow simulation. In practice, due to measurement uncertainty and riverbed erosion and deposition, river bathymetric errors are inevitable. Therefore, identifying major cross sections with large bathymetric errors is of great significance. In this study, forward and reverse flow routing models were developed and then applied to obtain two different water stages for a specific cross section, which were respectively propagated from the upstream and downstream boundaries. The spatial variation of differences between the two calculated water stages was compared to quantify the influence of bathymetric errors, and then used as an indicator for the location identification of the bathymetric errors. After being tested and verified in a hypothetical river case, the identification method was then applied to the Xunjiang River case. The results show that the proposed method can effectively identify the cross sections with large bathymetric errors, and the identification performance is related to the flow magnitude. The research is valuable and practical to the improvement of river bathymetric data and the accuracy of water flow simulation.

Key words: bathymetric error, inverse problem, location identification, reverse flow routing, river water stage

HIGHLIGHTS

- A location identification method for river bathymetric errors was proposed.
- The method identified single and multiple locations with bathymetric errors.
- The location identification results were affected by the flow magnitude.
- The research results are helpful for improving bathymetric data.

GRAPHICAL ABSTRACT

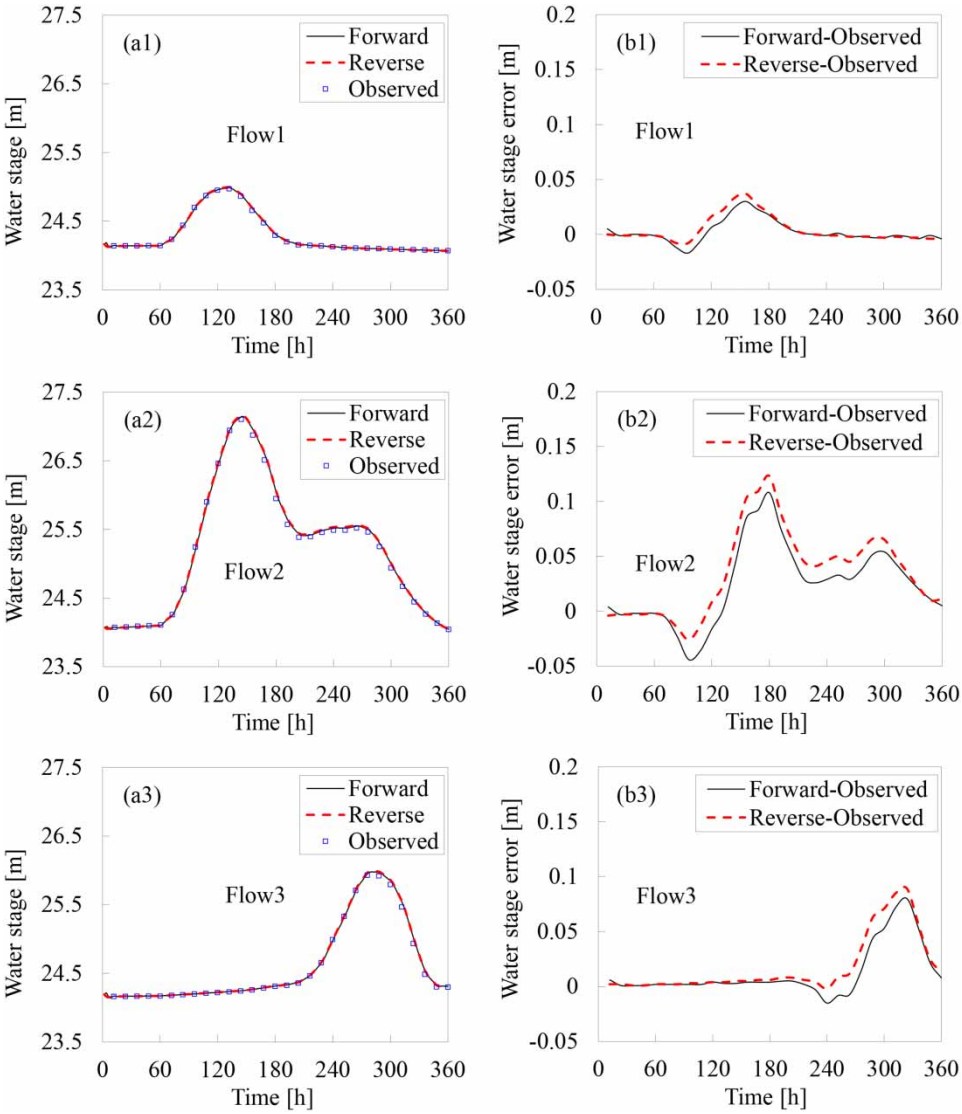

INTRODUCTION

River flow routing is a core issue in the flood control and water resource management. When using hydrodynamic flood routing models, the river bathymetric data is fundamental. Generally, the river bathymetric data derives from two sources (Luo *et al.* 2021): observations from field surveys, and integration data with postprocessing of bathymetric map and remote-sensing image as well as the digital elevation model (Liu *et al.* 2015). In practice, because of the high cost in time and labor and the difficulty in field surveys (Yu *et al.* 2014; Harada & Li 2018), the obtained bathymetric data are usually used over a long period. However, due to the measurement uncertainty and riverbed deformation, river bathymetric errors are inevitable. For example, the riverbed erosion and deposition at sharp river bends can significantly change the river morphology, and the sand mining usually deepens the water depth in a short time (Han *et al.* 2010). All these river morphological modifications induce large bathymetric errors to the flow routing. Recently, the above-mentioned issue has been widely studied, and a popular strategy to attenuate bathymetric errors is using data assimilation and data fusion with remote sensing images (Yoon *et al.* 2012; Wen *et al.* 2020), in which the variation of submerged topography cannot be identified. Therefore, it is of great significance to provide a method that can identify and then correct bathymetric data with large errors.

Research on the issue of river bathymetric errors at home and abroad is mainly concentrated on riverbed morphological modification (Byrnes *et al.* 2002; Zhang *et al.* 2002), the bathymetric data uncertainty assessment (Buhman *et al.* 2002; Harman *et al.* 2008), and the integration of multiple sources of topographic information (Shintani & Fonstad 2017; Luo *et al.* 2021), as well as the influence of bathymetric uncertainty on flood routing (McKean *et al.* 2014; Bures *et al.* 2019). Bailly *et al.* (2010) designed a methodology to assess the quality of LiDAR topographical data within rivers using a specific geostatistical method that conducts upscaling as well as interpolation of reference data. Cea & French (2012) estimated the influences of bathymetric error on the calibration and validation of estuarine data with a depth-averaged hydrodynamic model. Zhou *et al.* (2001) analyzed the abnormal water stage in some river sections of the Pearl River network, and found that river sand mining was mainly responsible for local bathymetric changes. McKean *et al.* (2014) compared flow model predictions using the lidar bathymetry with those made using a total station channel field survey and studied the effects of bathymetric lidar errors on flow properties. As the river topography directly determines the relationship between flow discharge and water stage, the disturbance of river topography can be reflected in the flow information. For example, Zhou *et al.* (2021) proposed a correction method of river bathymetry parameters based on stage–discharge rating curves as the rating curve represents the characteristics of the river section. Schaperow *et al.* (2019) used curve-fitting methods to predict unknown bathymetry with varying assumptions about height-width relationships. Nevertheless, the flow routing errors can only be calculated in those cross sections with observations, and there is still no feasible strategy to judge where the bathymetric error is located.

When the water flow is simulated at the cross section with large bathymetric errors, the difference between the flow information propagated from the upstream and reversely propagated from the downstream will be significant. This difference can be used to infer the bathymetric error. This study aims at proposing a method to identify the cross sections with large bathymetric errors, based on the forward and reverse flow routing. However, because the existing reverse flow routing models are mainly based on hydrological methods (Eli *et al.* 1974; D' Oria & Tanda 2012), they share the same shortcomings in the feasibility of water stage simulation, as well as a deficiency in model stability and accuracy (Guan *et al.* 2006; Szymkiewicz 2008). To overcome the shortcomings, this study first developed stable models for both the forward and reverse flow routing, supporting the numerical simulation of water stage in different directions for the bathymetric error identification.

The location identification method of river bathymetric errors is introduced in the methodology section. After being tested and demonstrated in a hypothetical case, the proposed identification method is applied to the case of the Xunjiang River in a real-world case study. Following the two cases, the proposed method is briefly discussed. Finally, conclusions are given in the last section.

METHODOLOGY

Forward flow routing model

The forward flow routing model in rivers was based on the one-dimensional Saint-Venant equations, which were derived from the conservation principles of mass and momentum, as follows:

$$B\frac{\partial Z}{\partial t}+\frac{\partial Q}{\partial x}=q \tag{1}$$

$$\frac{\partial Q}{\partial t}+\frac{\partial}{\partial x}\left(\frac{Q^2}{A}\right)+gA\frac{\partial Z}{\partial x}+g\frac{n_s^2Q|Q|}{AR^{\frac{4}{3}}}=0 \tag{2}$$

where x represents the location along the river [m], t represents the time [s], Q represents the flow discharge [m^3/s], Z represents the water stage [m], A represents the cross-sectional wetted area perpendicular to the river flow direction [m^2], q represents the lateral inflow within unit length along the flow direction [$m^3/(s{\cdot}m)$], g (=9.81 m/s^2) represents gravitational acceleration, n_s represents the riverbed roughness, and R represents the hydraulic radius [m].

In this study, the governing equations were discretized using the finite difference method. The discretization of time t and space x formed a grid on which the dynamical model was solved (see Figure 1) using approximations of the partial derivatives. Here, the implicit four-point Preissmann scheme was adopted because it allows non-equidistant grids and computes the discharge and stage at the same point (Chau 1990), as well as for its stability and convergence characteristics (Lyn & Goodwin

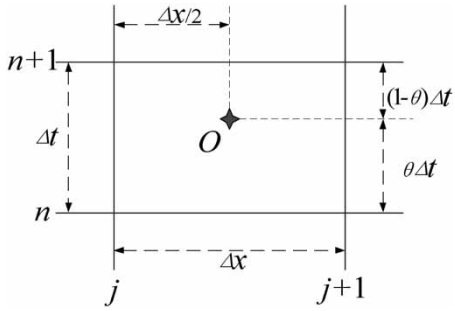

Figure 1 | Preissmann scheme using the finite difference method.

1987). The labels n and $n+1$ represent the previous and present time steps, respectively. The labels j and $j+1$ represent the adjacent grid points in the x direction.

The time- and space-dependent variables and their derivatives were discretized according to Figure 1 and have the forms of Equations (3)–(6):

$$f_O \approx \frac{\theta}{2}(f_{j+1}^{n+1} + f_j^{n+1}) + \frac{1-\theta}{2}(f_{j+1}^{n} + f_j^{n}) \tag{3}$$

$$\left.\frac{\partial f}{\partial t}\right|_O \approx \frac{f_{j+1}^{n+1} + f_j^{n+1} - f_{j+1}^{n} - f_j^{n}}{2\Delta t} \tag{4}$$

$$\left.\frac{\partial f}{\partial x}\right|_O \approx \theta\left(\frac{f_{j+1}^{n+1} - f_j^{n+1})}{\Delta x}\right) + (1-\theta)\left(\frac{f_{j+1}^{n} - f_j^{n})}{\Delta x}\right) \tag{5}$$

$$\left.\frac{\partial f^2}{\partial x}\right|_O \approx \theta\left(\frac{f_{j+1}^{n} f_{j+1}^{n+1} - f_j^{n} f_j^{n+1})}{\Delta x}\right) + (1-\theta)\left(\frac{f_{j+1}^{n} f_{j+1}^{n} - f_j^{n} f_j^{n})}{\Delta x}\right) \tag{6}$$

where Δx and Δt represent the time and space step sizes, respectively, θ is the weight coefficient between time steps ranging from 0 to 1 (Chau 1990), f is a generic flow variable, and the subscript O represents the currently calculated grid.

According to the discretization, the Saint-Venant equations were transformed into linear equations as follows:

$$a_{2j-1}^1 \Delta Q_j + a_{2j-1}^2 \Delta Z_j + a_{2j-1}^3 \Delta Q_{j+1} + a_{2j-1}^4 \Delta Z_{j+1} = b_{2j-1} \tag{7}$$

$$a_{2j}^1 \Delta Q_j + a_{2j}^2 \Delta Z_j + a_{2j}^3 \Delta Q_{j+1} + a_{2j}^4 \Delta Z_{j+1} = b_{2j} \tag{8}$$

where Q_j and Z_j represent the flow discharge and water stage at present time $n+1$ and at the j^{th} discrete cross section, respectively. Δ denotes the iterative increment of Q and Z. The coefficients a_{2j-1}^i, a_{2j}^i and b_{2j-1}, b_{2j} are determined by the

flow discharge and the water stage at time n ($i = 1, 2, 3, 4,\ j = 1, 2, \cdots$), as follows:

$$a^1_{2j-1} = -a^3_{2j-1} = -1;$$

$$a^2_{2j-1} = a^4_{2j-1} = \frac{B^*_{j+1/2}\Delta x}{2\Delta t\theta};$$

$$b_{2j-1} = \frac{\theta(q^{n+1}_j + q^{n+1}_{j+1}) + (1-\theta)(q^n_j + q^n_{j+1})}{2\theta}\Delta x - \frac{1-\theta}{\theta}(Q^n_{j+1} - Q^n_j) + a^2_{2j-1}(Z^n_j + Z^n_{j+1}) - (a^1_{2j-1}Q^*_j + a^2_{2j-1}Z^*_j + a^3_{2j-1}Q^*_{j+1} + a^4_{2j-1}Z^*_{j+1});$$

$$a^1_{2j} = \frac{\Delta x}{2\Delta t\theta} - \left(\frac{Q}{A}\right)^*_j + \left(g\frac{n^2|Q/A|}{2\theta R^{\frac{4}{3}}}\right)^*_j \Delta x;$$

$$a^2_{2j} = -a^4_{2j} = -g(A^*_j + A^*_{j+1})/2;$$

$$a^3_{2j} = \frac{\Delta x}{2\Delta t\theta} + \left(\frac{Q}{A}\right)^*_{j+1} + \left(g\frac{n^2|Q/A|}{2\theta R^{\frac{4}{3}}}\right)^*_{j+1} \Delta x;$$

$$b_{2j} = \frac{\Delta x}{2\Delta t\theta}(Q^n_{j+1} + Q^n_j) - \frac{1-\theta}{\theta}\left[\left(\frac{Q^2}{A}\right)^n_{j+1} - \left(\frac{Q^2}{A}\right)^n_j\right] + \frac{1-\theta}{\theta}a^2_{2j-1}(Z^n_{j+1} - Z^n_j) - (a^1_{2j}Q^*_j + a^2_{2j}Z^*_j + a^3_{2j}Q^*_{j+1} + a^4_{2j}Z^*_{j+1})$$

where B represents the top width of cross section [m]. * denotes the last iterative value of Q and Z.

Because of the hyperbolic nature of the Saint-Venant equations, boundary conditions are required (Singh 2004). In most river flood routing cases, the riverbed slope is small, and the flow state remains in the subcritical regime (Meselhe *et al.* 1997). Therefore, both the upstream and downstream boundary conditions are needed. Three types of boundary conditions are commonly used in the river flood routing: the time-variable discharge series, time-variable stage series, and stage-discharge rating curve or combined flow and stage hydrographs (Singh 2004; Lian *et al.* 2007). Generally, the time-variable inflow series is obtained and input into the flood routing model as the upstream boundary condition (Pappenberger *et al.* 2006), and the inflow propagation in the river is then simulated. For the downstream boundary condition, the time-variable stage series can be used if there are gauging stations at the outlet; otherwise, the stage-discharge rating curve is used when no stage observation is available (Schmidt & Yen 2008; Jung *et al.* 2018). In this research, the following boundary conditions were used:

$$Q_1 = Q_{up}(t) \tag{9}$$

$$Q_L = \alpha(Z_L + \beta)^\gamma \tag{10}$$

where α, β, and γ are constants and L represents the last river cross section.

Finally, the linear Equations (7) and (8) were solved using the double-sweep method, which is an efficient method for solving a set of linear algebraic equations (Zhang 2005).

Reverse flow routing model

Compared with forward flow routing, the reverse routing can be carried out in three different ways, namely, only reverse in space, only reverse in time, and reverse in both space and time (Eli *et al.* 1974), as shown in Figure 2. The forward model predicts the future states along the flow direction, while the reverse model traces the historical trajectory from downstream to upstream. In a numerical simulation, the reverse iteration to solve the Saint-Venant equations is usually unstable because of attenuation along the flow direction (sharpness in reverse). Therefore, most previous research on reverse flow routing shares the same instability issue, particularly for the way of reverse in both space and time (Figure 2(b)). In this study, the way of reverse in time but forward in space was also not considered because the upstream information is usually unknown in reverse flow routing (Figure 2(d)).

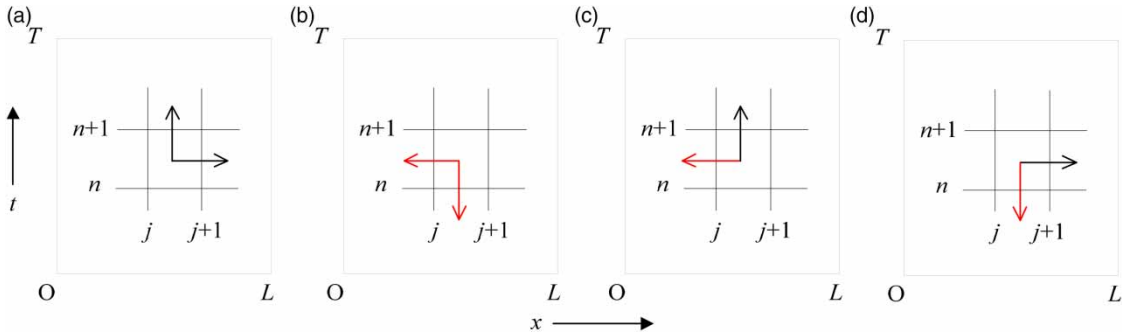

Figure 2 | Different reverse routing ways.

To improve model stability, an anticlockwise rotation transformation to the iteration direction of forward model was implemented to use the way of only reverse in space (see Figure 2(c), Figure 3).

After rotation transformation, the boundary and initial conditions of the forward model were switched to the initial and boundary conditions of the reverse model, respectively. The best contribution of this transformation is that the rotated numerical iteration to reversely solve the Saint-Venant equations is no longer in a negative direction of time or space (Figure 3), and therefore, improves the model stability (Wang *et al.* 2020). After the rotation transformation, the Saint-Venant equations were also transformed into linear equations in a different way, as follows:

$$a^1_{2n-1}\Delta Q^n + a^2_{2n-1}\Delta Z^n + a^3_{2n-1}\Delta Q^{n+1} + a^4_{2n-1}\Delta Z^{n+1} = b_{2n-1} \tag{11}$$

$$a^1_{2n}\Delta Q^n + a^2_{2n}\Delta Z^n + a^3_{2n}\Delta Q^{n+1} + a^4_{2n}\Delta Z^{n+1} = b_{2n} \tag{12}$$

where $\Delta Q^n = Q^n_j - Q^n_*$, $\Delta Z^n = Z^n_j - Z^n_*$, Q^n_*, Z^n_* are the iterative increments of Q^n_{j+1}, Z^n_{j+1}, coefficients a^i_{2n-1}, a^i_{2n} $(i = 1, 2, 3, 4)$ and b_{2n-1}, b_{2n} are calculated as follows:

$$a^1_{2n-1} = \frac{1-\theta}{\theta};\ a^3_{2n-1} = 1;$$

$$a^2_{2n-1} = -a^4_{2n-1} = \frac{B^{n+\theta}_* \Delta x}{2\Delta t\theta};\ B^{n+\theta}_* = \theta B^{n+1}_* + (1-\theta)B^n_*;$$

$$b_{2n-1} = -\frac{\theta(q^{n+1}_j + q^{n+1}_{j+1}) + (1-\theta)(q^n_j + q^n_{j+1})}{2\theta}\Delta x + Q^{n+1}_{j+1} + \frac{1-\theta}{\theta}Q^n_{j+1} + a^2_{2n-1}(Z^{n+1}_{j+1} - Z^n_{j+1}) - (a^1_{2n-1}Q^n_* + a^2_{2n-1}Z^n_* + a^3_{2n-1}Q^{n+1}_* + a^4_{2n-1}Z^{n+1}_*);$$

$$a^1_{2n} = \frac{\Delta x}{2\Delta t\theta} + \frac{1-\theta}{\theta}\left(\frac{Q}{A}\right)^*_j - \left(g\frac{1-\theta}{2\theta}\frac{n_s^2|Q/A|}{R^{\frac{4}{3}}}\right)^n_* \Delta x;$$

$$a^2_{2n} = gA^{n+\theta}_*\frac{1-\theta}{\theta};\ a^4_{2n} = gA^{n+\theta}_*;\ A^{n+\theta}_* = \theta A^{n+1}_* + (1-\theta)A^n_*;$$

$$a^3_{2n} = -\frac{\Delta x}{2\Delta t\theta} + \left(\frac{Q}{A}\right)^n_* - \left(g\frac{n_s^2|Q/A|}{2R^{\frac{4}{3}}}\right)^{n+1}_* \Delta x;$$

$$b_{2n} = \frac{\Delta x}{2\Delta t\theta}(Q^{n+1}_{j+1} - Q^n_{j+1}) + \left(\frac{Q}{A}\right)^{n+1}_* Q^{n+1}_{j+1} + \frac{1-\theta}{\theta}\left(\frac{Q}{A}\right)^n_* Q^n_{j+1} + gA^{n+\theta}_*\left(Z^{n+1}_{j+1} + \frac{1-\theta}{\theta}Z^n_{j+1}\right) + gn_s^2\frac{\Delta x}{2}\left[\left(\frac{|Q/A|}{R^{\frac{4}{3}}}\right)^{n+1}_* Q^{n+1}_{j+1} + \frac{1-\theta}{\theta}\left(\frac{|Q/A|}{R^{\frac{4}{3}}}\right)^n_* Q^n_{j+1}\right] + (a^1_{2n}Q^n_* + a^2_{2n}Z^n_* + a^3_{2n}Q^{n+1}_* + a^4_{2n}Z^{n+1}_*)$$

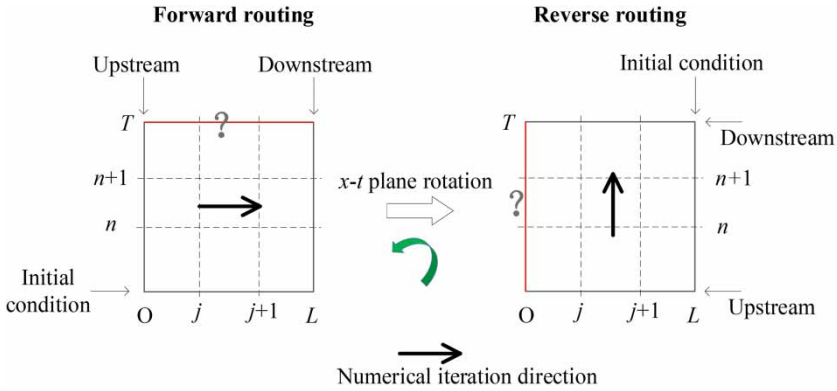

Figure 3 | Rotation transformation of the iteration direction of forward flow routing.

The linear Equations (11) and (12) were solved using the double-sweep method, after the boundary and initial conditions respectively obtained from the initial and boundary conditions of the forward flow routing model. The difference between the forward and reverse flow routing models are compared in Table 1.

Location identification of bathymetric errors

For every cross section input to the flow routing models, its bathymetric error can be reflected by the flow simulation results. Actually, it was found that the disturbance caused by the bathymetric error has significant influences on the simulated water stage. Moreover, the influence of this disturbance can be judged by the difference between the water stages respectively obtained from the forward and the reverse flow routing models. Looking at the cross section with large bathymetrical errors (for example, the j^{th} cross section), the water stage at this location obtained from the forward model is denoted as $Z1_j^n$, and the water stage obtained from the reverse model is denoted as $Z2_j^n$. Then, the location of bathymetric errors can be identified with the difference between $Z1_j^n$ and $Z2_j^n$, which is quantified by the indicator dif_Z_j, estimated as follows:

$$dif\_Z_j = \frac{1}{T}\left(\sum_{n=1}^{T} Z1_j^n - \sum_{n=1}^{T} Z2_j^n\right) \tag{13}$$

where $n = 1, 2, \cdots, T$, T is the total computational time.

According to Equation (13), the dif_Z_j at different locations can be calculated. Then, the cross section with large bathymetric errors can be identified, since dif_Z_j at this location is much larger than its adjacent cross sections with no or small bathymetrical errors.

HYPOTHETICAL CASE STUDY

In this study, the proposed method was firstly examined with it applied to a prismatic trapezoidal river, whose detailed information is as follows: a bottom width of 30 m, a side slope of 2.5, a bottom slope of 0.0001, and a roughness coefficient of 0.017. The river length is 20 km, and the gauging station is located at 16 km away from the river inlet. The study explores

Table 1 | Comparison between the forward and reverse flow routing model (Wang *et al*. 2020)

Comparison item	Forward flow routing	Reverse flow routing
Numerical scheme	Implicit four-point Preissmann scheme	Implicit four-point Preissmann scheme
Direction of flow simulation	Forward both in time and space	Reverse in space and forward in time
Variables to be solved	$\Delta Q_j, \Delta Z_j, \Delta Q_{j+1}, \Delta Z_{j+1}$	$\Delta Q^n, \Delta Z^n, \Delta Q^{n+1}, \Delta Z^{n+1}$
State updating	From time n to $n+1$	From cross section $j+1$ to j
Initial condition	$t = 0,\ x = 0,\ 1,\ \ldots, L$	$x = L,\ t = 0, 1,\ \ldots, T$
Boundary conditions	Upstream: $x = 0,\ t = 0, 1,\ \ldots, T$ Downstream: $x = L,\ t = 0, 1,\ \ldots, T$	Upstream: $t = 0,\ x = 0,\ 1,\ \ldots, L$ Downstream: $t = T,\ x = 0,\ 1,\ \ldots, L$

the scenarios in which there are bathymetric errors in the riverbed elevation, side slope and bottom width, at a single cross section (5 km and 10 km away from the river inlet, respectively) or at multiple cross sections. In the reverse flow routing, the gauging cross section was taken as the starting calculation section from downstream to upstream, and the flow and water stage hydrograph at this location is shown in Figure 4.

At first, the water stage simulated respectively by the forward and reverse routing models were compared in Figure 5, without any bathymetric error considered. In Figure 5, the time before the flow peak ($t = 24$ h), around flow peak ($t = 36$ h), and after flow peak ($t = 48$ h) were presented. According to the comparisons, the simulated water stages from two routing models are very close to each other. However, due to the model uncertainty, there still exists some differences between the water stages from two models, with the maximum value about 0.03 m, although no bathymetric error considered.

Natural rivers are frequently modified by human activities. For example, the sand mining can deepen the riverbed elevation. Therefore, this study considered several scenarios with bathymetric errors including the decrease of the riverbed elevation, the decrease of the side slope, and the increase of the bottom width. To distinguish with the influence of model uncertainty, this study compared the variation of dif_Z_j in the case with no bathymetric errors. The test results are shown in Figures 6 and 7.

In Figures 6(a) and 7(a), it can be found that the model uncertainty induces obvious water stage errors, and a maximum value about 0.005 m of dif_Z_j can be observed when no bathymetric error is considered. However, different from this kind of continuous and smooth variations by the model itself, the variation of dif_Z_j in the case with bathymetric errors shows an abrupt change. At the location of 5 km or 10 km with bathymetric errors, the corresponding dif_Z_j is significantly abnormal, and this cross section can be identified according to the anomalies of abrupt change.

Due to frequent human activities, it's likely that multiple cross sections of natural rivers undergo significant bathymetric modifications at the same time (Zang *et al.* 2020). To further examine the practicability of the identification method, the variation of dif_Z_j in the cases with bathymetrical errors at two or three cross sections was analyzed, as shown in Figures 8 and 9.

The results in Figures 8 and 9 also verify the model performance, as it can also identify multiple locations with large bathymetric errors. In addition, if the large bathymetric error is located at the gauging cross section, it can be directly judged by comparing the simulations from the forward model and the observations at this location.

REAL-WORLD CASE STUDY

After being tested in the hypothetical case, the proposed location identification method was then applied to the Xunjiang River case to further demonstrate its feasibility. The main reach of the Xunjiang River from the Dahuangjiangkou gauging station to the Tengxian gauging station (96.19 km away from the Dahuangjiangkou station) was selected for the case study. The bathymetric data used for identification came from 27 cross sections measured in 2011 (Table 2). The measured data were spatially interpolated and input into the river flow calculation models with the uniform space step 500 m. The river location and its gauging stations are shown in Figure 10.

To analyze the influence of flow patterns, three different flow hydrographs since 2016 (Figure 11) were selected for comparison. The water stage observations were available at Pingnan, the other gauging station along this study river, and were used to verify the simulations from the two models, as shown in Figure 12.

The results in Figure 12 indicate that the simulated water stages from two models were very close to the observations with small errors. It can be found that the simulations from the forward model were slightly better than that from the reverse

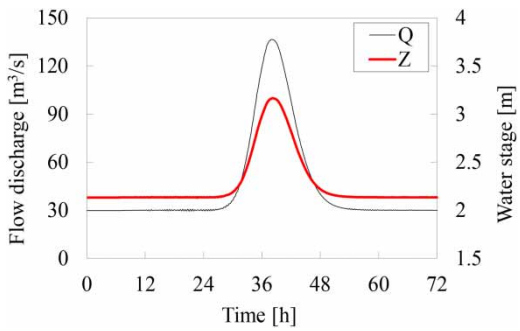

Figure 4 | Observations at the gauging station.

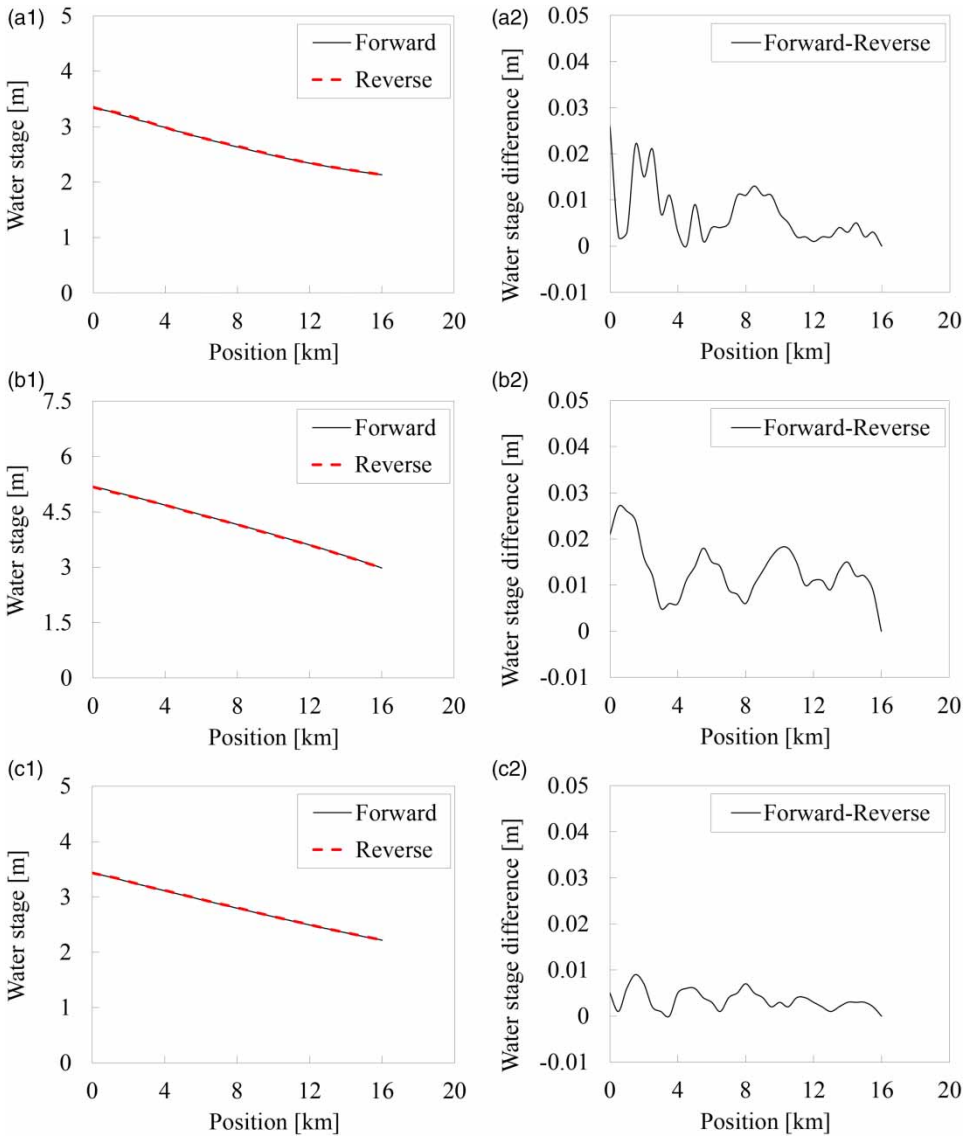

Figure 5 | Water stages simulated respectively by the forward and reverse routing models and their difference along river. The left column shows water stages and the right column shows their difference.

model. Nevertheless, when only a single model (forward routing model or reverse routing model) was used, it could be difficult to judge the location of bathymetric errors. For the cross section with flow routing results compared to the observations, the time-variation of simulation errors was almost in accordance with the observed water stage while the information of bathymetric error was not reflected.

After model verification, the location identification method was then applied to the three selected flows, and the results are shown in Figure 13.

In Figure 13, there are significant anomalies in the spatial variation of dif_Z_j around Mengjiangkou (ID 20, 73.89 km). The identification results indicate that there should be a large bathymetric error around the Mengjiangkou cross section, which was likely to be caused by the scour and deposition of its tributary, Mengjiang River. In addition, comparing the results of three flows in Figure 13, it can be found that the abrupt change of dif_Z_j is closely related to the flow magnitude. Generally, the spatial variation of dif_Z_j is more significant in the larger flow case. Similarly to the hypothetical river case, the dif_Z_j at the upper river reach is larger than that at the lower reach, and the dif_Z_j tends to decrease along the river, which might be attributed to the effects of boundary conditions.

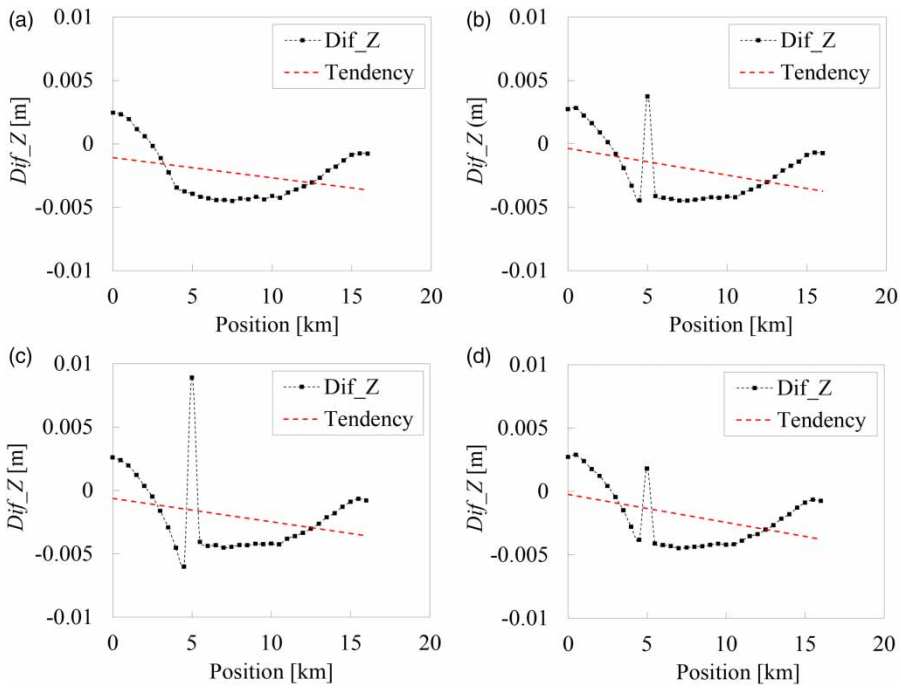

Figure 6 | Variation of dif_Z_j along the river in the case of bathymetric errors located at 5 km away from the river inlet. (a) No bathymetric errors, (b) the bottom width was decreased by 10 m, (c) the riverbed elevation was decreased by 0.2 m, (d) the side slope was changed to 4.0.

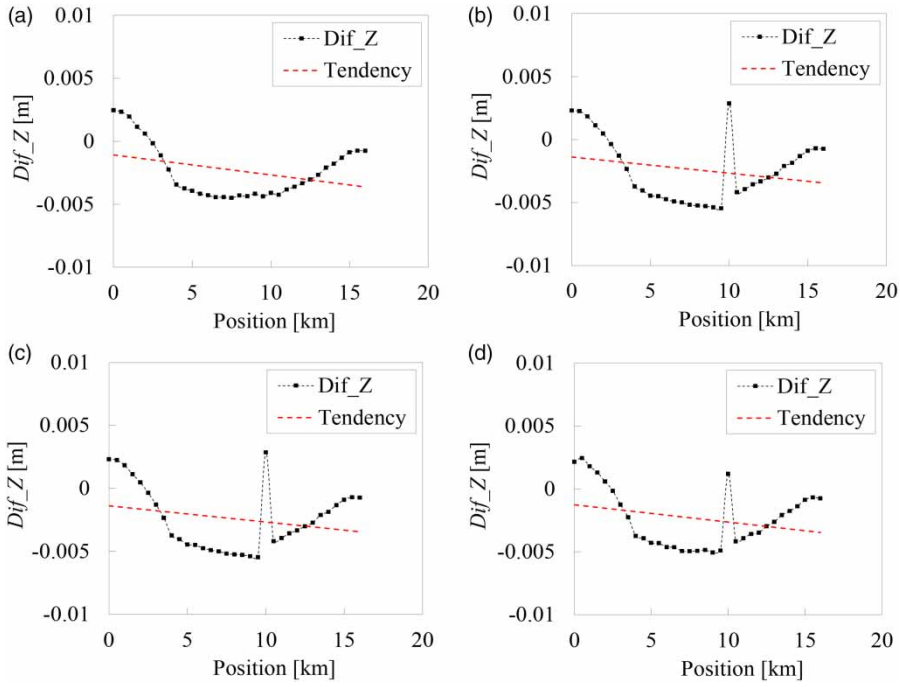

Figure 7 | Variation of dif_Z_j along the river in the case of bathymetric errors located at 10 km away from the river inlet. (a) No bathymetric errors, (b) the bottom width was decreased by 10 m, (c) the riverbed elevation was decreased by 0.2 m, (d) the side slope was changed to 4.0.

Due to the irregular hydraulic geometry of this natural river, the variation of dif_Z_j were much more dramatic, resulting in that the bathymetric error identification was worse than the hypothetical case, especially for the case with small flow magnitude. Therefore, when using the proposed identification method, a flow with a larger magnitude is suggested to be selected. Overall, the proposed method in this study is feasible for the location identification of bathymetric errors in a natural river.

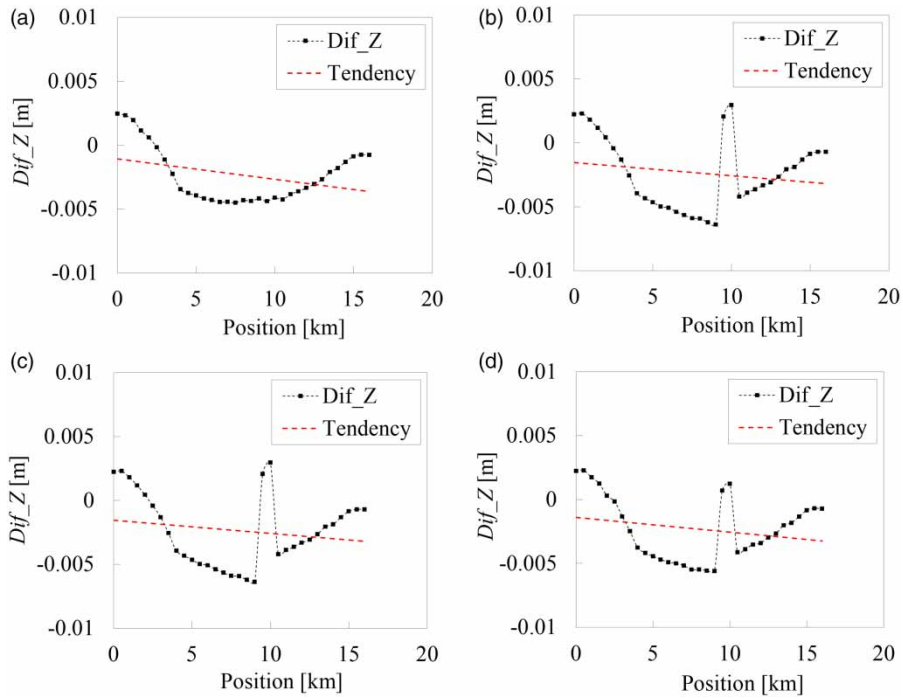

Figure 8 | Variation of *dif_Z*$_j$ along the river in the case of bathymetric errors located at two points around 10 km away from the river inlet. (a) No bathymetric errors, (b) the bottom width was decreased by 10 m, (c) the riverbed elevation was decreased by 0.2 m, (d) the side slope was changed to 4.0.

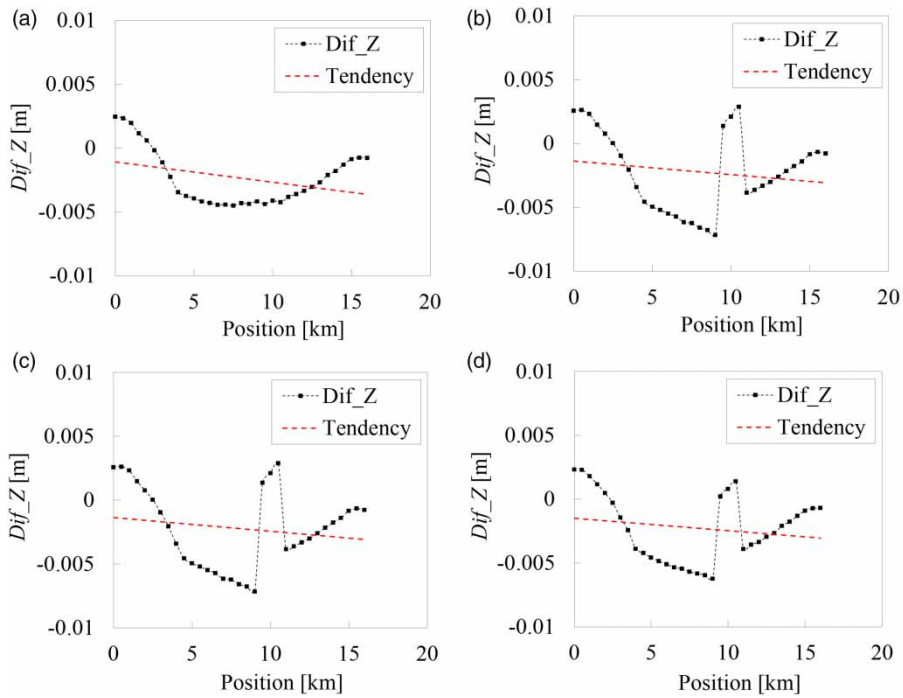

Figure 9 | Variation of *dif_Z*$_j$ along the river in the case of bathymetric errors located at three points around 10 km away from the river inlet. (a) No bathymetric errors, (b) the bottom width was decreased by 10, (c) the riverbed elevation was decreased by 0.2 m, (d) the side slope was changed to 4.0.

Table 2 | The cross sections of Xunjiang River measured in 2011

ID	Name	Position [km]	ID	Name	Position [km]
1	Dahuangjiangkou	0	15	Longshigou	53.49
2	Walingding	6.08	16	Jiudiling	59.12
3	Xiangsizhou	9.61	17	Dangzhou	66.29
4	Sijie	12.11	18	Fozidong	69.20
5	Guyong	14.76	19	Tangchongdukou	71.39
6	Shangchong	17.76	20	Mengjiangkou	73.89
7	Pingnanmucai Plant	23.09	21	Xiajun	78.99
8	Pingnan	26.04	22	Silizhou	81.44
9	Suhetang	28.53	23	Dengzhou	88.05
10	Pingnan fertilizer plant	33.53	24	Niuerchongkou	88.75
11	Dacheng	35.63	25	Shangdengjian	90.47
12	Sanhexiang	41.43	26	Xialing	92.37
13	Danzhuwei	44.03	27	Tengxian	96.19
14	Changqitang	45.58			

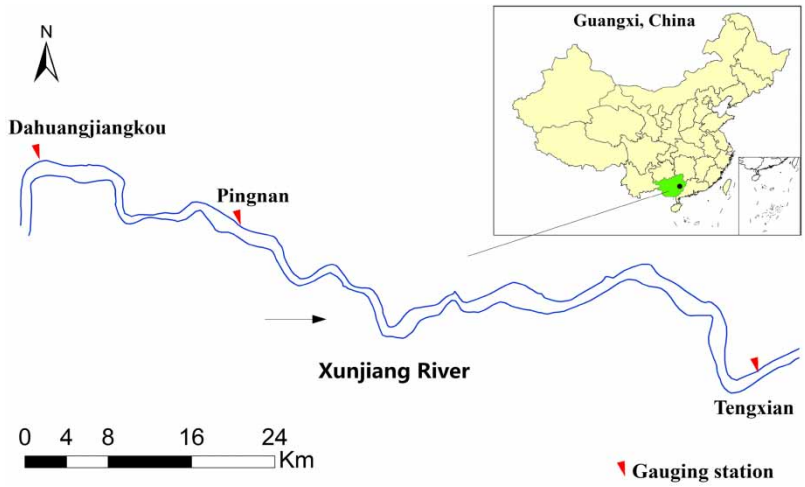

Figure 10 | Locations of Xunjiang River and its gauging stations.

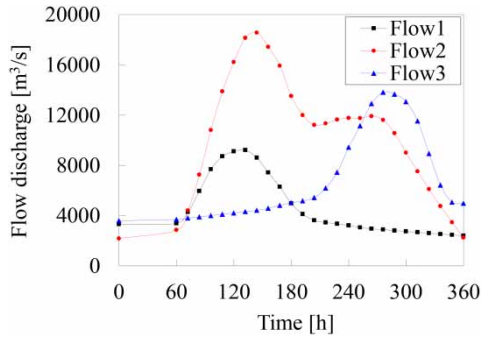

Figure 11 | Three floods observed at Dahuangjiangkou in 2016.

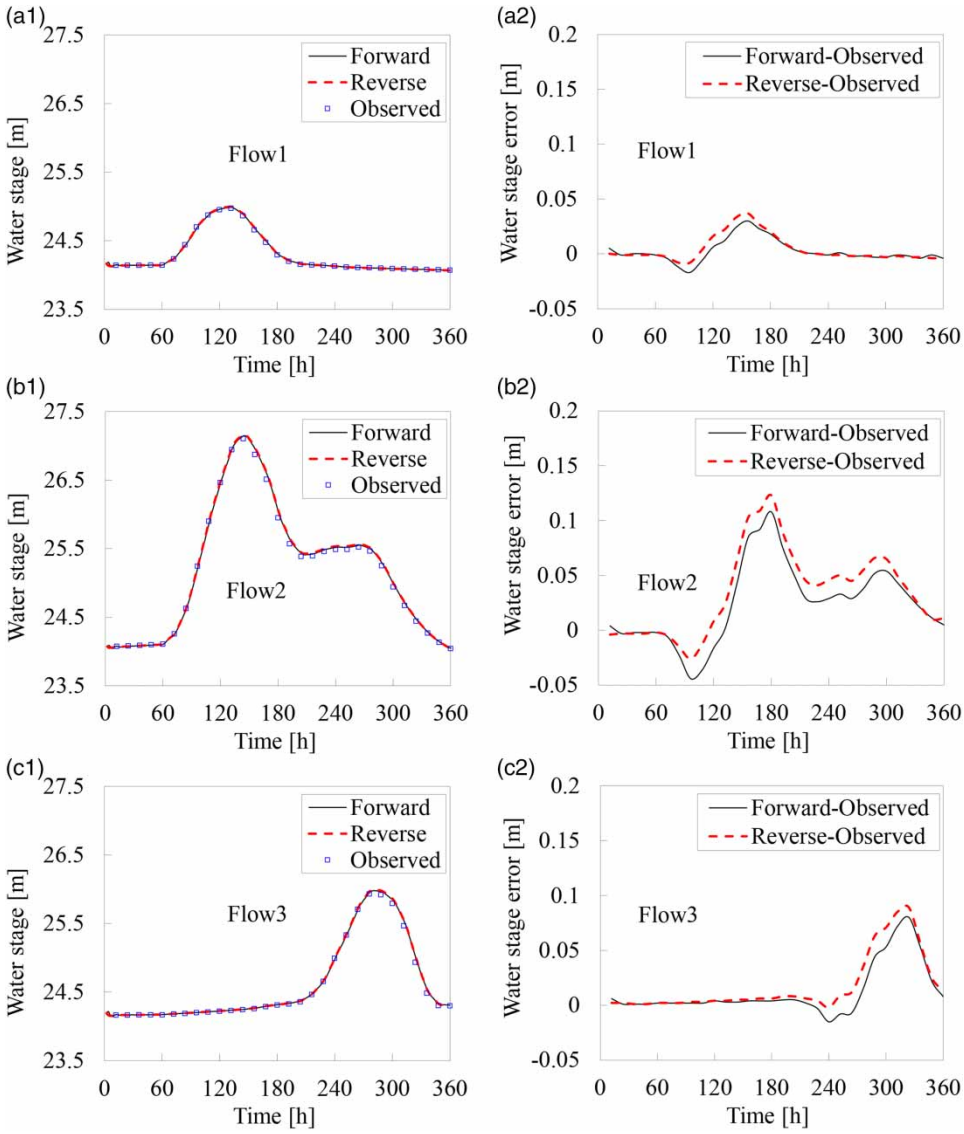

Figure 12 | Model verification with the observed water stage at Pingnan.

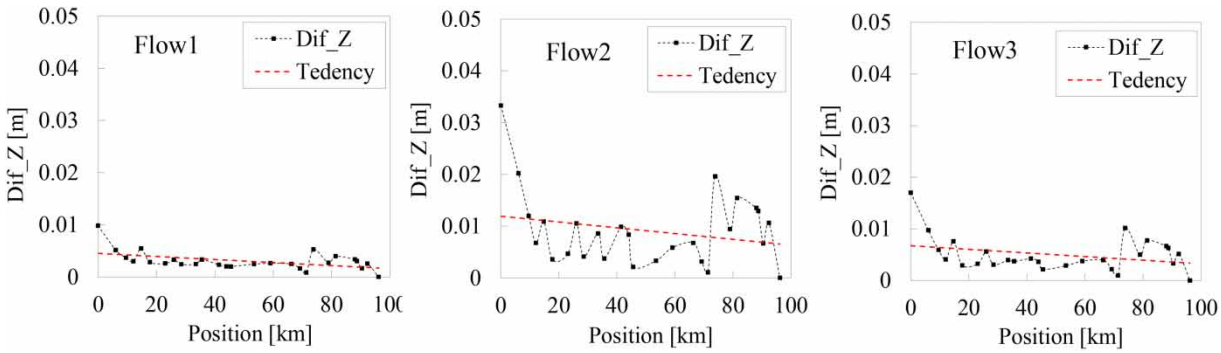

Figure 13 | Variation of *dif_Z*$_j$ along the river in the real-world river case.

DISCUSSION

The proposed location identification method was successfully applied to a hypothetical and a real-word river case, and the cross sections with large bathymetric errors could be picked out according to the spatial variation of dif_Z_j along the river. Nonetheless, several points should be discussed to better understand the identification method.

(1) In Figures 6–9 and 13, the maximum dif_Z_j respectively caused by model uncertainty and bathymetric error were close to each other. However, the spatial variations were significantly different. Different from the continuous and smooth variations by model itself, the variation of dif_Z_j by bathymetric error presented an abrupt change. Thus, the identification was mainly determined by the spatial variation rule of dif_Z_j, although its performance was affected by flow magnitude, which was quite different in the two cases.

(2) In the hypothetical case, the abrupt change of dif_Z_j caused by bottom width, bottom elevation and slope deformation could not be distinguished in Figures 6–9. The identification method itself was also not able to determine the detailed reason for bathymetric error. In the real-world case, after the location identification, the possible reasons for bathymetric error can be further analyzed by integration with field surveys, as well as the remote sensing images. After identification, the subsequent work to improve the bathymetric data as well as the flow simulation is also important. The idea of data assimilation using EnKF (Wang *et al.* 2019) associated with field surveys will be tried in our following studies.

(3) Compared with previous works on this topic, the main contribution of this study is to put forward an identification indicator dif_Z_j, whose spatial variation along the river can partition the effects respectively from model uncertainty and bathymetric error. And the developed flow routing models that can well simulate the water stage made the calculation of dif_Z_j feasible. Although the adopted numerical schemes are closely related to the calculation of dif_Z_j, the identification results are not affected by the selected simulation methods, because the abrupt change of dif_Z_j attributed to bathymetric error can be judged as long as the models can well simulate the water stage in both forward and reverse directions.

CONCLUSIONS

In this research, a method for identifying the river bathymetric error location was proposed, based on the forward and reverse flow routing. This study first built the forward and reverse flow routing models, and then quantified the influence of the river bathymetric errors on water flow simulation according to the variation characteristics of simulated water stage. The identification indicator dif_Z_j was calculated, using the water stage respectively obtained from the forward and the reverse flow routing models, and the location of bathymetric errors was then determined.

The proposed method was examined by a hypothetical river case and then applied to a real-world river case. The main conclusions are given as follows: (1) For the hypothetical river, the method effectively identified single and multiple locations with bathymetric errors in the riverbed elevation, bottom width and side slope. (2) In the case of the natural river, the identification results were affected by the flow magnitude. Generally, the spatial variation of dif_Z_j was more significant in the larger flow case. Nonetheless, the proposed method in this study was feasible for the location identification of bathymetric error in a natural river. (3) When using the proposed identification method, a flow with larger magnitude is suggested to be selected. (4) The proposed method can effectively identify the location of river bathymetric errors, and the research results are helpful for improving the bathymetric data and the accuracy of water flow simulation.

ACKNOWLEDGEMENTS

This work was supported by the Guangdong Basic and Applied Basic Research Foundation (2020A1515110906), the National Natural Science Foundation of China (52109047), and the Joint Open Research Fund Program of State Key Laboratory of Hydroscience and Engineering and Tsinghua – Ningxia Yinchuan Joint Institute of Internet of Waters on Digital Water Governance (sklhse-2021-Iow01).

We would like to offer thanks for the review work by the editors and the anonymous reviewers.

CONFLICT OF INTEREST STATEMENT

The authors declare no conflicts of interest.

DATA AVAILABILITY STATEMENT

All relevant data are included in the paper or its Supplementary Information.

REFERENCES

Bailly, J. S., Le Coarer, Y., Languille, P., Stigermark, C. J. & Allouis, T. 2010 Geostatistical estimations of bathymetric LiDAR errors on rivers. *Earth Surface Processes and Landforms* **35** (10), 1199–1210.

Buhman, D. L., Gates, T. K. & Watson, C. C. 2002 Stochastic variability of fluvial hydraulic geometry: Mississippi and Red rivers. *Journal of Hydraulic Engineering* **128** (4), 426–437.

Bures, L., Roub, R., Sychova, P., Gdulova, K. & Doubalova, J. 2019 Comparison of bathymetric data sources used in hydraulic modelling of floods. *Journal of Flood Risk Management* **12**, e12495.

Byrnes, M. R., Baker, J. L. & Li, F. 2002 Quantifying potential measurement errors and uncertainties associated with bathymetric change analysis. In: *Engineer Research and Development Center Vicksburg Ms Coastal and Hydraulics Lab*.

Cea, L. & French, J. R. 2012 Bathymetric error estimation for the calibration and validation of estuarine hydrodynamic models. *Estuarine, Coastal and Shelf Science* **100**, 124–132.

Chau, K. W. 1990 Application of the Preissmann scheme on flood propagation in river systems in difficult terrain. *Hydrology in Mountainous Regions. I-Hydrological Measurements. IAHS Publ.* **193**, 535–543.

D'Oria, M. & Tanda, M. G. 2012 Reverse flow routing in open channels: a Bayesian geostatistical approach. *Journal of Hydrology* **460**, 130–135.

Eli, R. N., Wiggert, J. M. & Contractor, D. N. 1974 Reverse flow routing by the implicit method. *Water Resources Research* **10** (3), 597–600.

Guan, Z., Wu, H., Cu, J., Deng, L. & Zhao, M. 2006 A study on back mathematical calculation procedure of Muskingum method. *Journal of China Hydrology* **26** (2), 9–12. (in Chinese).

Han, Z., Tian, X. & Ou, S. 2010 Impacts of large-scale human activities on riverbed morphology and tidal dynamics at Modaomen estuary. *Scientia Geographica Sinica* **30** (04), 582–587. (in Chinese).

Harada, S. & Li, S. S. 2018 Combining remote sensing with physical flow laws to estimate river channel geometry. *River Research and Applications* **34** (7), 697–708.

Harman, C., Stewardson, M. & DeRose, R. 2008 Variability and uncertainty in reach bankfull hydraulic geometry. *Journal of Hydrology* **351** (1-2), 13–25.

Jung, J. Y., Niemann, J. D. & Greimann, B. P. 2018 Modeling input errors to improve uncertainty estimates for one-dimensional sediment transport models. *Stochastic Environmental Research and Risk Assessment* **32** (6), 1817–1832.

Lian, Y., Chan, I. C., Singh, J., Demissie, M., Knapp, V. & Xie, H. 2007 Coupling of hydrologic and hydraulic models for the Illinois River Basin. *Journal of Hydrology* **344** (3-4), 210–222.

Liu, C., Xin, X. & Yin, W. 2015 Method of extracting river cross section data based on DEM. *Yangtze River* **46** (S1), 9–11. (in Chinese).

Luo, Q., Zhang, H., Wang, Z. & Kang, X. 2021 River channel bathymetric mapping based on multi-technology fusion: method and practice. *Tropical Geomorphology* **42** (01), 36–40. (in Chinese).

Lyn, D. A. & Goodwin, P. 1987 Stability of a general Preissmann scheme. *Journal of Hydraulic Engineering* **113** (1), 16–28.

McKean, J., Tonina, D., Bohn, C. & Wright, C. W. 2014 Effects of bathymetric lidar errors on flow properties predicted with a multi-dimensional hydraulic model. *Journal of Geophysical Research: Earth Surface* **119** (3), 644–664.

Meselhe, E. A., Sotiropoulos, F., Holly, J.- & M, F. 1997 Numerical simulation of transcritical flow in open channels. *Journal of Hydraulic Engineering* **123** (9), 774–783.

Pappenberger, F., Matgen, P., Beven, K. J., Henry, J., Pfister, L. & Fraipont, P. 2006 Influence of uncertain boundary conditions and model structure on flood inundation predictions. *Advances in Water Resources* **29** (10), 1430–1449.

Schaperow, J. R., Li, D., Margulis, S. A. & Lettenmaier, D. P. 2019 A curve-fitting method for estimating bathymetry from water surface height and width. *Water Resources Research* **55** (5), 4288–4303.

Schmidt, A. R. & Yen, B. C. 2008 Theoretical development of stage-discharge ratings for subcritical open-channel flows. *Journal of Hydraulic Engineering* **134** (9), 1245–1256.

Shintani, C. & Fonstad, M. A. 2017 Comparing remote-sensing techniques collecting bathymetric data from a gravel-bed river. *International Journal of Remote Sensing* **38** (8–10), 2883–2902.

Singh, V. P. 2004 Flow routing in open channels: some recent advances. Notes downloaded from the site http://www. riverflow2004. unina. it (Date of access: February 14, 2010).

Szymkiewicz, R. 2008 Application of the simplified models to inverse flood routing in upper Narew river (Poland). *Publications of the Institute of Geophysics, Polish Academy of Sciences* **EG9** (405), 121–135.

Wang, J., Zhao, J., Lei, X. & Wang, H. 2019 An effective method for point pollution source identification in rivers with performance-improved ensemble Kalman filter. *Journal of Hydrology* **577**, 123991.

Wang, J., Zhao, J., Lei, X., Wang, H. & Liao, W. 2020 Reverse flow routing in rivers on the rotated x-t plane. *Journal of Tsinghua University (Science and Technology)* **60** (10), 855–863. (in Chinese).

Wen, K., Li, Y., Wang, H., Yang, J., Jing, W. & Yang, C. 2020 Estimating inland water depth based on remote sensing and machine learning technique. *Tropical Geography* **40** (2), 314–322. (in Chinese).

Yoon, Y., Durand, M., Merry, C. J., Clark, E. A., Andreadis, K. M. & Alsdorf, D. E. 2012 Estimating river bathymetry from data assimilation of synthetic SWOT measurements. *Journal of Hydrology* **464**, 363–375.

Yu, Q., Chen, Y. & Zhu, D. 2014 River cross-section extraction from DEM for one-dimensional hydrodynamic modeling. *Journal of Hydroelectric Engineering* **33** (03), 133–137 + 157. (in Chinese).

Zang, Z., Li, J., Liu, F. & Yang, Q. 2020 Responses of channel evolution to human interventions in the West River Network. *Journal of Sediment Research* **45** (03), 61–66. (in Chinese).

Zhang, Y. 2005 Simulation of open channel network flows using finite element approach. *Communications in Nonlinear Science & Numerical Simulation* **10** (5), 467–478.

Zhang, X., Tan, G., Xu, Q. & Shi, G. 2002 Model for predicting cross section deformation of river channel based on BP neural networks. *Journal of Hydraulic Engineering* **11** (8), 2. (in Chinese).

Zhou, Z., Luo, X., Luo, Z. & Yang, Q. 2001 The analysis on the major reason about local exceptional rise of flood water level in the Pearl River delta in recent years. *Tropical Geography* **04**, 319–322. (in Chinese).

Zhou, X., Revel, M., Modi, P., Shiozawa, T. & Yamazaki, D. 2021 Correction of river bathymetry parameters using the stage–discharge rating curve. *researchgate.net*.

First received 4 March 2022; accepted in revised form 31 March 2022. Available online 11 April 2022